Journal of Materials Chemistry A

ROYAL SOCIETY OF CHEMISTRY

PAPER

View Article Online
View Journal | View Issue

Cite this: J. Mater. Chem. A, 2021, 9, 11073

Metal-doped bipyridine linked covalent organic framework films as a platform for photoelectrocatalysts†

Tomoya Hosokawa,[a] Masaki Tsuji,[a] Kosei Tsuchida,[a] Kazuyuki Iwase,[bc] Takashi Harada,[b] Shuji Nakanishi *[abd] and Kazuhide Kamiya *[abd]

Received 15th January 2021
Accepted 5th April 2021

DOI: 10.1039/d1ta00396h

rsc.li/materials-a

The development of efficient photoenergy conversion systems is highly demanded from the viewpoint of solving energy and environmental problems. Covalent organic frameworks (COFs) have attracted much attention as novel photofunctional materials because of their wide-range visible-light absorption, which is related to their large π-conjugation systems. The other important property of COFs is their ability to support a wide variety of metals *via* coordinate bonds; metal-doped COFs exhibit various electron-transfer catalytic activities depending on the metal species. Here, we newly synthesized free-standing metal-doped COF films as photoelectrocatalysts and evaluated the photoelectrochemical oxygen reduction reaction (ORR) properties of Cu atoms doped in a COF. The photocurrent corresponding to the ORR started to increase under 670 nm irradiation, and the photocurrent for the Cu-doped COF was five times larger than that for the COF without Cu. The action spectra, fluorescence spectra, and *in situ* X-ray absorption spectra indicate that the electrons photoexcited in the COF were transferred to oxygen *via* the Cu atoms. Thus, the Cu atoms coordinated to the COF serve as active catalytic sites for the photoinduced ORR.

Introduction

Covalent organic frameworks (COFs), which are crystalline cross-linked microporous polymers, have received considerable research interest as a novel polymeric platform because of their unique physicochemical properties including high robustness, nanoporous structure, and high design flexibility.[1–5] In addition to these advantages, COFs exhibit wide-range visible-light absorption because of their large π-conjugation systems.[6–8] Thus, COFs are expected to be developed as next-generation photofunctional materials.[7–13] For example, highly crystalline sulfone-containing COFs modified with Pt nanoparticles exhibit high activity toward photochemical hydrogen evolution (as high as 16.3 mmol g^{-1} h^{-1}).[14] Metal-free carbazole-triazine-based COFs, which have a narrow bandgap of 2.04 eV, have been found to promote photocatalytic carbon dioxide (CO_2) reduction to carbon monoxide (CO) under visible-light irradiation.[15]

Another attractive property of COFs is their ability to immobilize single metal atoms *via* coordinate bonds with abundant heteroatoms with a lone electron pair, such as N, S, and O, and to exhibit unique functions derived from metal centers, similar to homogeneous organometallics.[16–26] That is, the use of COFs is a novel approach to achieve heterogeneous single-atom catalysts as the analogues of homogeneous organometallics. For example, Ding *et al.* have reported that a Pd-modified imine-linked COF catalyzes coupling reactions with high robustness and easy recyclability.[27] Gunasekar *et al.* showed that Ir-modified triazine-linked COFs catalyze highly efficient carbon dioxide hydrogenation and exhibit high stability in air.[28] In addition to these thermocatalytic properties of metal-doped COFs (M-COFs), several groups including us have recently demonstrated that M-COFs exhibit various unique electrocatalytic functions depending on the metal species.[29–35,78] Cu- and Ni-doped COFs, for example, function as electrocatalysts for the oxygen reduction reaction (ORR) and carbon dioxide reduction reaction (CRR), respectively.[18,33] In our catalysts, the adsorption energy of the substrates or key intermediates adsorbed onto the metal atoms in COFs can be precisely tuned through fine control of the coordination environment, leading to unique reaction activity and selectivity.

Considering electron-transfer catalytic ability that depends on their metal centers and wide-range visible-light absorption,

[a]Graduate School of Engineering Science, Osaka University, 1-3 Machikaneyama, Toyonaka, Osaka 560-8531, Japan. E-mail: kamiya@chem.es.osaka-u.ac.jp; nakanishi@chem.es.osaka-u.ac.jp

[b]Research Center for Solar Energy Chemistry, Osaka University, 1-3 Machikane-yama, Toyonaka, Osaka 560-8531, Japan

[c]Institute of Multidisciplinary Research for Advanced Materials (IMRAM), Tohoku University, 2-1-1 Katahira, Aoba-ku, Sendai, Miyagi 980-8577, Japan

[d]Innovative Catalysis Science Division, Institute for Open and Transdisciplinary Research Initiatives (ICS-OTRI), Osaka University, Suita, Osaka 565-0871, Japan

† Electronic supplementary information (ESI) available. See DOI: 10.1039/d1ta00396h

metal-modified COFs are expected to be an attractive platform for materials for photoelectrochemical applications. However, the general process to fabricate COF electrodes is to paste the nanopowders on conductive substrates using organic binders, which are basically insulative and scatter and/or absorb irradiated light.[36–39] To tackle this obstacle, we attempted to utilize free-standing films of COFs as binder-free photoelectrocatalysts.[40–48] In the present work, we here newly synthesized free-standing metal-doped bipyridine-linked COF (bpy-COF) films and applied them as binder-free photoelectrocatalysts. The details of the photoinduced charge transfer process were investigated using photoelectrochemical action spectra, photoluminescence spectra, and *in situ* spectroscopy by employing the ORR mediated by Cu sites doped in the bpy-COF (Cu-bpy-COF).

Results and discussion

The targeted reaction system

We first explain in detail the photoelectrochemical ORR using Cu-bpy-COF films and why they were chosen as the representative reaction system of the M-COF photoelectrocatalysis in the present work. The photoinduced ORR is an attractive and well-studied process as the cathodic reaction of light-driven fuel cells or rechargeable metal–air batteries and as a method for the photosynthesis of hydrogen peroxide.[49–54] Especially, the ORR in neutral solutions has attracted keen attention for application in enzymatic and microbial fuel cells.[55] Imine- and bpy-linked COFs were adopted as the backbone structure of organic frameworks because single metal centers can be immobilized at the bipyridine moiety through coordinate bonds. Especially, free-standing films of bpy-COFs will provide a unique approach to developing binder-free photoelectrochemical devices.[56–59] In a previous paper, we used first-principles calculations to demonstrate that coordinatively unsaturated Cu sites in bpy-COFs facilitate the electrochemical ORR.[33,60] Thus, the single Cu sites coordinated with the bipyridine moiety are expected to possess unsaturated coordination environments and efficiently catalyze the ORR.

Physical and morphological characterization of COF films

The bpy-COF films were synthesized by oil/water interfacial synthesis using an aqueous solution of 2,2-bipyridine-5,5′-diamine (upper layer, 0.70 mmol L^{-1}) and a dichloromethane solution of 2,4,6-triformylphloroglucinol (Tp) (lower layer, 0.75 mmol L^{-1}).[56] The polymerization spontaneously proceeded at the oil/water interface at 30 °C for 72 h. We then impregnated the resulting film with 5 mM $CuCl_2$ aqueous solution to dope Cu^{2+} ions into the bpy-COF film (Cu-bpy-COF) (Fig. 1a). Fig. 1b shows images of the bpy-COF and Cu-bpy-COF, respectively. The orange transparent bpy-COF film (2 cm × 2 cm) turned reddish after the impregnation, which suggests that Cu atoms were successfully doped into the bpy-COF (for the details in reddish color, see Fig. 3). N_2 isotherm analysis of the bpy-COF was performed at 77 K to analyze its pore structure (Fig. S1a†). A typical type-I isotherm was observed, indicating the existence of

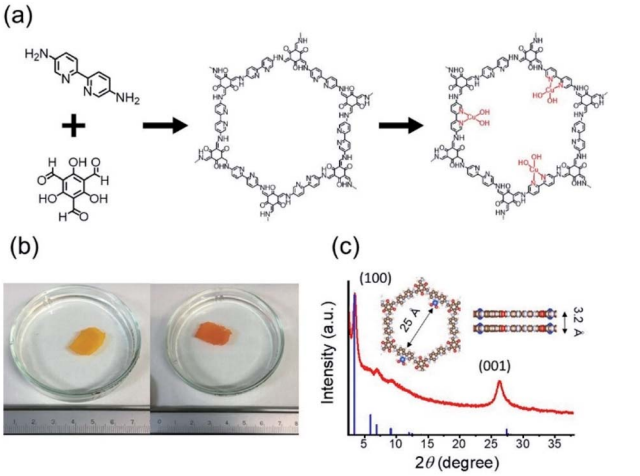

Fig. 1 (a) Schematic illustration of the synthesis of the Cu-bpy-COF film. (b) Photographs of the free-standing bpy-COF (left) and the Cu-bpy-COF (right) films. (c) Experimentally (red) and simulated (blue) obtained X-ray diffraction patterns of the Cu-bpy-COF film and the eclipsed structure of Cu-bpy-COF. C: brown, O: red, N: silver, H: pale, and Cu: blue.

micropores with 1.2–2.1 nm (Fig. S1b†), as reported in the previous papers.[56,61,62] The Brunauer–Emmett–Teller (BET) specific surface area was 1270 m^2 g^{-1}, which basically corresponded to the surface area of bpy-COF powder.[56] The morphology was characterized by scanning electron microscopy (SEM) and atomic force microscopy (AFM). The AFM height histogram of the bpy-COF (Fig. S2†) indicates that the average thickness of the bpy-COF was approximately 400 nm. Needle-like COF crystallites were observed in the high-magnification SEM image (Fig. S3†), consistent with the results reported in the previous paper.[56]

We physically characterized the Cu-bpy-COF using various X-ray techniques. The X-ray diffraction (XRD) pattern of the Cu-bpy-COF shows peaks at $2\theta = 3.5°$ and 26.5°, which are assigned to the (100) and (001) planes of the Cu-bpy-COF, respectively (Fig. 1c). These XRD patterns indicate that the bpy-COF has an eclipsed structure (Fig. 1c), consistent with the previously reported structure for the bpy-COF.[56,62] Notably, the characteristic peaks at $2\theta = 7.5°$ and 14° assigned to the staggered stacking are almost negligible.[52]

Table S1† lists the surface elemental compositions calculated by X-ray photoelectron spectroscopy (XPS). The atomic ratio of the Cu atoms in the Cu-bpy-COF was 1.8%, and the Cu/N ratio was 0.13. In addition, the Cu amount evaluated by the ICP was 1.1 at%, which is about two-thirds of the value obtained by XPS. Thus, the Cu concentration in the near-surface was a little higher than that in the bulk. We analyzed the Cu 2p XPS and X-ray absorption near edge structure (XANES) spectra to determine the oxidation states of the Cu atoms. The Cu $2p_{3/2}$ XPS peaks generated by the Cu-bpy-COF at 932.7 eV correspond to Cu(II) ions (Fig. S4†).[63] The Cu K-edge XANES spectra of Cu metal, Cu_2O, and CuO are shown in Fig. 2a. The absorption edge of the Cu-bpy-COF was 8980 eV, which is similar to that of

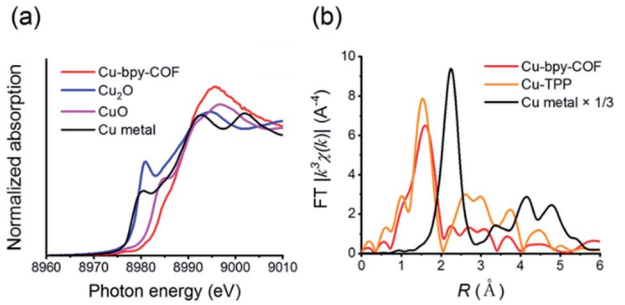

Fig. 2 (a) Cu–K edge XANES spectra and (b) k^3-weighted Fourier transform of EXAFS spectra for the Cu–K edge of the Cu-bpy-COF (red), Cu_2O (blue), CuO (pink), Cu foil (black), and Cu TPP (orange).

CuO. These results indicate that the Cu(II) oxidation state was dominant in the Cu-bpy-COF. The Fourier transformations of the k^3-weighted EXAFS oscillations for the Cu-bpy-COF, Cu-5,10,15,20-tetraphenyl-21*H*,23*H*-porphine (Cu-TPP), and Cu metal are shown in Fig. 2b. The Cu–N peak for the Cu-bpy-COF is clearly observed at 1.6 Å, respectively. In contrast, peaks corresponding to Cu–Cu bonds (2.2 Å) and Cu–O–Cu bonds (2.7 Å) were not detected.[33] The EXAFS results indicate that the Cu atoms in the Cu-bpy-COF are individually isolated and anchored onto the bpy-COF through coordination with N atoms

Band structure of the Cu-bpy-COF

Here, the energy band structures of the COFs are investigated. The diffuse reflectance spectra of the Cu-bpy-COF and bpy-COF are shown in Fig. 3a. The absorption intensity of the bare bpy-COF begins to increase at 700 nm, corresponding to the π–π* transition of the bpy-COF (for details, see DFT calculation results). The bandgap calculated from the Tauc plot is 2.25 eV (Fig. 3b). We calculated the band structure of the Cu-bpy-COF using density functional theory (DFT) methods. Fig. 3c shows the density of states of the Cu-bpy-COF and bpy-COF. The bandgap of the bpy-COF, as determined from the DFT calculations, is 1.5 eV. Notably, the bandgap calculated using the generalized gradient approximation (GGA) is known to be underestimated.[64,65] The valence-band maximum (VBM) and conduction-band minimum (CBM) are composed of C 2π and C 2π* orbitals, respectively. Cu 3d orbitals are located in the bandgap of the Cu-bpy-COF, indicating that the photoexcited electrons in the conduction band can be thermodynamically transferred to Cu sites. On the basis of the DFT results, the new absorption at 700–800 nm in the spectrum of the Cu-bpy-COF is assigned to the Cu(II) d–d transition and/or the direct charge transfer transition from the VB to Cu(II).[66–68] We next carried out electrochemical measurements in an organic electrolyte to determine the absolute band position of the bpy-COFs.[69–72] The cyclic voltammograms of the bpy-COF films in acetonitrile containing 0.1 M tetrabutylammonium tetrafluoroborate (Bu_4NBF_4) are shown in Fig. S5.† The CBM of the bpy-COF was −0.77 V *vs.* the normal hydrogen electrode (NHE), calculated from the threshold of the cyclic voltammograms. The band structures of the bpy-COF determined on the basis of the UV-vis, cyclic voltammetry (CV), and DFT results are shown in Fig. S6.†

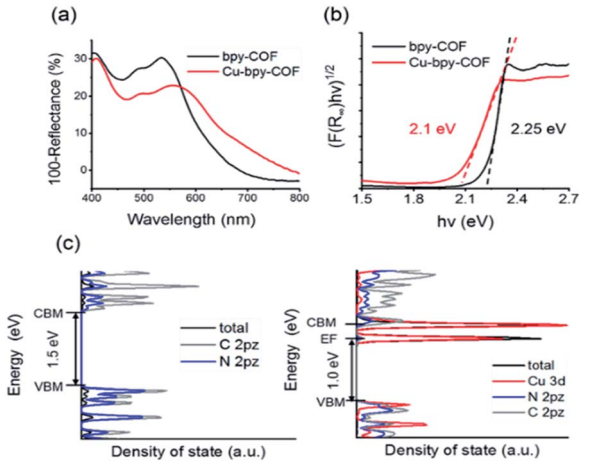

Fig. 3 (a) UV-vis diffuse reflection spectra (100 − reflectance/%) of bpy-COF and Cu-bpy-COF films. (b) Tauc plots of the Cu-bpy-COF and bpy-COF. (c) Total density of states (DOS) and partial density of states (PDOS) of the bpy-COF (left) and Cu-bpy-COF (right). Black, red, blue, and pink lines represent the DOS of all, C, N, and Cu, respectively.

(Photo)electrocatalytic activity of the Cu-bpy-COF

We evaluated the electrochemical ORR activity of the Cu-bpy-COF under dark conditions. A transparent conductive oxide film (indium-doped tin oxide, ITO) was coated with the Cu-bpy-COF as a working electrode without a binder (Fig. S7†). The roughness factor ($R_f = 1.62$) for the Cu-bpy-COF film calculated from the electrochemically accessible surface area (EASA) was similar to that for the reported powder Co-bpy-COF electrode[16] (for details, see Fig. S8a–c† and its caption). Changes in the current density (j) at different potentials (U) were examined for the Cu-bpy-COF, bpy-COF, and a bare ITO electrode in O_2-saturated 0.1 M phosphate buffer solution (pH 7.0) (Fig. S8d†). The ORR onset potential for the Cu-bpy-COF was −0.15 V *vs.* Ag/AgCl, which is approximately 300–500 mV more positive than the value associated with the bpy-COF or the bare ITO electrode.

The origin of the catalytic site for the ORR on the Cu-bpy-COF was examined using DFT calculations. The Gibbs free energy changes (ΔG) at 0.62 V *vs.* computational hydrogen electrode (CHE), which are associated with the formation of OOH*, OH*, and O*, are shown in Fig. S9.† The overall reaction pathway of the Cu-bpy-COF becomes exergonic, whereas the first electron transfer process (OOH* formation) is endergonic for the bare bpy-COF. Thus, the Cu site can reduce the activation barrier for the first electron transfer to O_2 molecules to form OOH*. Although Cu-macrocycles such as Cu-porphyrins or –phthalocyanines are known to exhibit poor ORR activity because of weak OOH* adsorption, the lower N coordination to Cu atoms in the Cu-bpy-COF than in Cu-macrocycles would lead to stronger adsorption of OOH and a lower ΔG, as demonstrated in the previous papers.[60,73]

Next, we evaluated the photoelectrochemical ORR properties of the Cu-bpy-COF. The photocurrents were measured under monochromated light using the electrochemical cell shown in Fig. S10.† Fig. S11† shows the representative photocurrent *vs.* time curve at −0.2 V and 0.2 V *vs.* Ag/AgCl under 650 nm light.

The cathodic current clearly appeared under visible-light irradiation. The apparent photocurrent was observed under even 650 nm irradiation, indicating that our M-COF film can utilize almost all visible light regions. The photocurrent action spectra, which represent the incident-photon-to-current-efficiency (IPCE) (λ), were then examined to obtain conclusive evidence of the origin of the photoresponse (Fig. 4a). Interestingly, Fig. 4a shows that the deposition of Cu into the bpy-COF drastically increased (by more than fivefold) the cathodic photocurrent. The IPCE for the Cu-bpy-COF started to increase under 670 nm irradiation, which clearly corresponds to the absorption spectrum of the Cu-bpy-COF. These results clearly indicate that the photocurrent originated from the photoabsorption of the Cu-bpy-COF. We observed the stable photocurrent for over 30 min (Fig. S12a†), suggesting that the cathodic current originated from the ORR, not from the degradation of COFs. In addition, we also measured the Fourier transform infrared (FT-IR) spectra of Cu-bpy-COF films before and after the photoelectrochemical test for 30 min (Fig. S12b†). The peaks assignable to C–N, C=C and C=O were observed, which corresponded to the reported data for the bpy-COF.[56,62] Notably, the change in the spectrum was not observed after a 30 min photoelectrochemical test. The stable photocurrent response and this FT-IR spectrum suggested that our bpy-COF is stable under photoelectrochemical conditions within this time scale. Fig. 4b shows the potential dependence of IPCE for the Cu-bpy-COF. The change in the polarity of photocurrent occurred at 0 V *vs.* RHE. In the more positive region, the anodic photocurrent was also enlarged in the presence of Cu in a similar manner to the cathodic photocurrent (Fig. S13†).

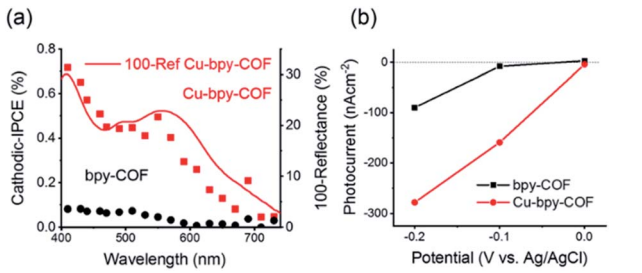

Fig. 4 (a) Action spectrum for the cathodic IPCE of the Cu-bpy-COF (red dots) and COF (black dots), and the absorption spectrum of the Cu-bpy-COF (solid red line) at −0.2 V *vs.* RHE in the presence of O_2. (b) Potential dependence of the value of photocurrent of the bpy-COF (black dots) and Cu-bpy-COF (red dots). These photocurrent responses were measured under the constant potentials. The photocurrent in (a) and (b) was obtained under the irradiated light shown in Fig. S10b and c,† respectively.

Photoinduced charge transfer pathway in Cu-bpy-COF films

We subsequently investigated the electron transfer mechanism of the Cu-bpy-COF in the presence of O_2 using photoluminescence spectroscopy and *in situ* XANES. Fig. 5a shows the photoluminescence spectra of the bpy-COF and Cu-bpy-COF excited by 380 nm radiation. Fluorescence quenching was clearly observed after the addition of Cu into the bpy-COF, which indicates that the excited electrons quickly transferred to Cu(II); thus, charge separation efficiently occurred.[74] Photoinduced charge transfer was also confirmed by gas-phase *in situ* XANES. The Cu-bpy-COF was placed in an X-ray-transparent plastic bag filled with Ar gas (Fig. S14†), and the XANES spectra were acquired under visible-light irradiation (Fig. 5b). When the sample was irradiated, the Cu–K absorption edge shifted to the lower-energy region (curve (1) to (2) in Fig. 5b), corresponding to

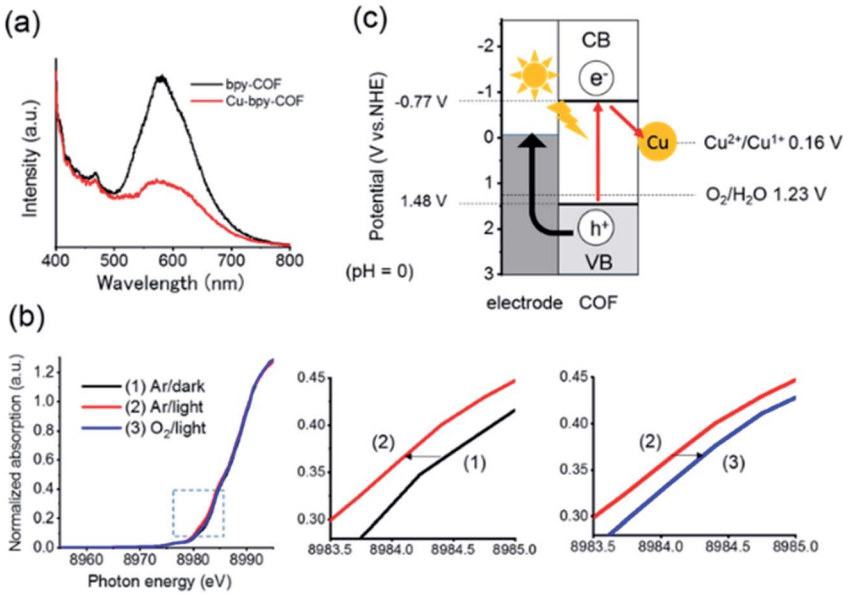

Fig. 5 (a) Photoluminescence spectra (λ_{exc} = 380 nm) of the bpy-COF (black) and Cu-bpy-COF (red). (b) Cu K-edge XANES spectra under Ar/dark (1, black), Ar/light (2, red), and O_2/light (3, blue). (c) The proposed photoinduced electron transfer process at the Cu-bpy-COF under visible-light irradiation.

a lower oxidation state of the Cu species. Approximately 3.4% of the Cu(II) ions were likely reduced to Cu(I) (see the section of the band structure of the Cu-bpy-COF).[67] After the sample was exposed to air (*i.e.*, O_2), the spectrum recovered to the initial state (curve (2) to (3) in Fig. 5b), indicating that Cu(II) was regenerated by the ORR. Photoelectrochemical measurements, photoluminescence, and *in situ* XANES analyses clearly show that the photoexcited electrons in the bpy-COF were transferred to O_2 molecules *via* the Cu atoms, as shown in Fig. 5c. The remaining holes in the VBs reached the ITO electrode, generating the cathodic photocurrent. Besides, the direct charge transfer transition from the VB to Cu(II) might occur to some extent in the longer wavelength region (see the section of the band structure of the Cu-bpy-COF). In addition, although the anodic photocurrent observed at more positive potentials than 0 V is outside the scope of the present paper, its mechanism might be explained as follows: when the applied potential was more positive than the Cu(I/II) redox potential, the photogenerated electrons in Cu sites were transferred to the ITO electrode more rapidly than to O_2 molecules.

Conclusions

We newly synthesized metal-modified bpy-COF films and applied the Cu-doped COF as a photoelectrocatalyst for the ORR. The synthesized COF showed absorption over the entire visible-light region (to 750 nm). The cathodic photocurrent attributed to the ORR was clearly observed for the COF films, and the current was drastically enhanced by the addition of Cu into the pores of the COFs. The photoluminescence and *in situ* X-ray absorption spectra indicated that the excited electrons were rapidly transferred to Cu sites and consumed by O_2 reduction. This work is the first demonstration of the potential for COF-based films to serve as photoelectrocatalysts. Given that M-COFs can exhibit various unique electron-transfer catalytic properties depending on their metal center, the M-COF films are potentially a novel polymeric platform for photoelectrocatalysts toward artificial photosynthesis. Furthermore, free-standing films will provide us with novel artificial photosynthesis systems. For example, the laminated heterojunction of anodic and cathodic M-COF films like the membrane electrode assembly (MEA) could be used as an all-solid-state Z-scheme laminated photocatalyst.[75] Such MEA-type photocatalysts would separately evolve CRR products and O_2 molecules as products of water oxidation.

Experimental

Synthesis of Cu-doped bpy-COF (Cu-bpy-COF) films

The bpy-COF films were synthesized *via* liquid–liquid interfacial synthesis using the reported method with a slight modification using 2,4,6-triformylphloroglucinol (Tp) (TCI) and 5,5′-diamino-2,2′-bipyridine (bpy) which were prepared by ourselves (see ESI for details†) as monomers.[56] Tp (15.7 mg) dissolved in dichloromethane (100 mL) was poured into a glass beaker. A spacer layer of water (60 mL) was gently added on top of the Tp solution. Finally, bpy (20.8 mg) and amine-*p*-toluene sulfonic acid monohydrate salt (*p*-TsOH) (38.7 mg) dissolved in water (100 mL) were added slowly on top of the spacer solution over a period of 30 min. The resultant bpy-COF film was washed with distilled water. The Cu-doped bpy-COF (Cu-bpy-COF) film was synthesized by a simple impregnation method by dipping a bpy-COF film into a Cu-ion solution. Cu was impregnated into the bpy-COF film for 12 h at room temperature using 5 mM $CuCl_2$ aqueous solutions. The resultant Cu-bpy-COF films were washed with distilled water twice and then dried under air.

Physical characterization

X-ray photoelectron spectra (Axis Ultra, Kratos Analytical) were acquired with monochromated Al Kα X-rays at $h\nu = 1486.6$ eV. The binding energies were calibrated using the C 1s peak at 284.8 eV. For calculation of the atomic concentration, backgrounds of core-level spectra were subtracted using the Shirley method. Inductively coupled plasma optical emission spectroscopy (ICP-OES) measurements were performed using an Optima 8300 (PerkinElmer). The fluorescence spectra of the synthesized bpy-COF film on a transparent slide glass were recorded using a spectrofluorometer (FP-8500, JASCO). Field-emission scanning electron microscopy (FE-SEM) experiments were carried out on a SU-8000 (Hitachi). The N_2 adsorption–desorption isotherms at 77 K were obtained using a 3 Flex (Micromeritics). The prepared bpy-COF film was ground into a fine powder in a mortar before measurement. Prior to the adsorption measurements, fine powder of the bpy-COF was degassed at 120 °C for 12 h under dynamic vacuum (1×10^{-4} Pa). The powder X-ray diffraction (XRD) patterns of the samples were obtained on an X'PERT-PRO diffractometer (PANalytical) using Cu Kα radiation ($l = 1.54$ Å, 45 kV, 40 mA). The data were collected over the 2θ range from 2.5° to 40° at a speed of 1° min^{-1}. UV-visible diffuse-reflectance spectra were obtained in diffuse reflectance mode at room temperature using a UV-vis spectrometer (U-4100, Hitachi) with an integrating sphere. Barium sulfide was used as a reference and standard sample. X-ray absorption fine structure (XAFS) spectra were obtained using the BL01B1 beamline at the Spring-8 facility of the Japan Synchrotron Radiation Research Institute (JASRI). Double-crystal Si (111) monochromators were used to obtain XAFS data. The measurements for as-prepared Cu-bpy-COFs were conducted in the fluorescence-yield mode using 19 elements of Ge solid-state detectors. Reference XAFS spectra were collected in transmission mode. Extended X-ray absorption fine structure (EXAFS) spectra were analyzed using the ATHENA software package. The FT-IR experiments were conducted in transmission mode using a Cary 670 FTIR (Agilent). The prepared Cu-bpy-COF film before and after the 30 minute photocurrent measurements was ground into a fine powder with KBr powder in a mortar before measurements.

Evaluation of the HOMO/LUMO energies of the bpy-COF film

Cyclic voltammograms in organic electrolytes were obtained using a standard one-compartment, three-electrode electrochemical cell. The Ag/Ag^+ electrode and Pt wire were used as reference and counter electrodes, respectively. A bpy-COF film

supported on a glassy carbon (GC) electrode was used as the working electrode. 0.1 M tetrabutylammonium hexafluorophosphate (Sigma-Aldrich) solution in acetonitrile was used as the electrolyte. The potential range was set between −2.5 V and 0.5 V, and the scan rate was 50 mV s^{-1}. The ferrocenium/ferrocene (Fc/Fc^{+}) redox potential was measured at the end to calibrate the Ag/Ag^{+} electrode. The lowest unoccupied molecular orbital (LUMO) of the bpy-COF was calculated using eqn (1) and (2):

$$E_{\mathrm{LUMO}}\ (\mathrm{eV}) = (E_{[\mathrm{onset,red}\ vs.\ \mathrm{Fc/Fc+}]} + 5.1) \quad (1)$$

$$E_{\mathrm{LUMO}}\ (\mathrm{eV}) = (E_{[\mathrm{onset,red}\ vs.\ \mathrm{NHE}]} + 4.75) \quad (2)$$

The highest occupied molecular orbital (HOMO) was estimated by the bandgap energies obtained from the UV-vis reflectance spectra. First, we transformed the absorption spectra by applying the Kubelka–Munk function ($F(R^{\infty})$) *via* eqn (3):

$$F(R^{\infty}) = \frac{K}{S} = \frac{(1-R^{\infty})^2}{2R^{\infty}} \quad (3)$$

where $R^{\infty} = R_{\mathrm{sample}}/R_{\mathrm{standard}}$. K and S are the absorption and scattering coefficients, respectively. The bandgap energy was obtained from the Tauc plot transformed according to eqn (4):

$$(F(R^{\infty})h\nu)^{\frac{1}{2}} = B(h\nu - E_{\mathrm{g}}) \quad (4)$$

where h is Planck's constant, ν is the photon frequency, E_g is the bandgap energy, and B is a constant.

Details for calculating the portions of Cu(II) reduced to Cu(I) by visible light irradiation

Normalized absorbance (μ_N) was calculated by $\mu_N = \ln(I_0/I)$, where I_0 is the intensity of the incident X-rays, and I is that of the fluorescent X-rays. Here, the μ_N values at 8980 eV were 0.08578, 0.06318, and 0.5815 in the presence of the Cu(II)-bpy-COF before reaction, Cu(II)-bpy-COF during reaction under Ar and visible light irradiation, and Cu_2O, respectively. Thus, eqn (5) is valid:

$$0.06318 = \ln\left(\frac{I_0}{I_{(\mathrm{II})}}\right), 0.5815 = \ln\left(\frac{I_0}{I_{(\mathrm{I})}}\right),$$

$$0.08578 = \ln\frac{I_0}{\alpha I_{(I)} + (1-\alpha)I_{(II)}} \quad (5)$$

where $I_{(II)}$ and $I_{(I)}$ are the intensities of the fluorescent X-rays in the presence of Cu(II) and Cu(I), respectively, and a is the portion of Cu(II) converted to Cu(I). In this way, α was calculated to be 0.0342 (3.4%).

(Photo)electrochemical measurements

A double-chamber electrochemical cell and an electrochemical measurement system (HZ-5000, Hokuto Denko) equipped with a three-electrode system were used to evaluate the electro- or photoelectrocatalytic activity of the M-bpy-COFs. The geometrical surface area of the electrode was 0.50 cm^2. Ti wire and Ag/AgCl (KCl sat.) were used as the counter and reference electrodes, respectively. The anodic and cathodic compartments were separated by a Nafion membrane. The working electrodes were prepared by placing the bpy-COF films on transparent conductive electrodes. The electrodes were washed with boiled acetone for 30 min and then sonicated in water for 30 min before use.

Oxygen reduction reaction

The electrochemical ORR activity was investigated under 1 atm O_2 conditions in a 0.1 M phosphate buffer solution (pH 7.0). Before reduction, O_2 gas was bubbled for 30 min. The scan rate for the current–voltage curves was 100 mV s^{-1}.

All measured potentials were converted to E(RHE) using eqn (6):

$$E(\mathrm{V}\ vs.\ \mathrm{RHE}) = E(\mathrm{V}\ vs.\ \mathrm{Ag/AgCl}) + 0.197 + 0.059 \times \mathrm{pH} \quad (6)$$

The incident-photon-to-current-efficiency (IPCE) is defined as eqn (7):

$$\mathrm{IPCE}(\%) = \frac{1}{P} \times \frac{1240}{\lambda} \times 100 \quad (7)$$

where I is the photocurrent density (mA cm^{-2}), P is the intensity of the light irradiated onto the working electrode (mW cm^{-2}), and λ is the wavelength (nm). I was calculated using eqn (8):

$$I = I_{\mathrm{L}} - I_{\mathrm{D}} \quad (8)$$

where I_L is the average light current density for the first 1 min and I_D is the average dark current density just before the light irradiation.

The IPCE was measured using light (400–780 nm in 20 nm increments) from a Xe lamp (LA-410UV-3, HAYASHI-REPIC) passing through a band-pass filter (half-width = 10 nm, Asahi Spectra). The IPCE was measured under an applied potential at −0.2 V and +0.2 V *vs.* Ag/AgCl in 0.1 M phosphate buffer solution (pH 7.0). The potential dependence of the value of photocurrent was measured under visible light (λ > 650 nm) using a Xe lamp (LA-410UV-3, HAYASHI-REPIC) with a long-wave pass filter (LV0650 Asahi Spectra).

Computational details

We carried out density functional theory (DFT) calculations for the ORR activity of the Cu-bpy-COF using the OpenMX code.[76,77] The generalized gradient approximation of the Perdew–Burke–Ernzerhof model (GGA-PBE) was used. The kinetic cut-off energy was selected at 120 Ryd, and the vacuum layer was set to be greater than 15 Å; (2 × 2 × 1) k-points were used. We calculated all atoms within the relaxations in all directions. The atomic relaxations were conducted until the maximum force on any atom was less than 10^{-4} Hartree $Bohr^{-1}$.

For the electrocatalytic ORR process, the model of the computational hydrogen electrode was used to calculate the energy of a proton–electron pair, where the energy of a proton–electron pair was approximated as one-half of the free energy of

H_2 molecule under standard conditions.[60] The Gibbs free energy (ΔG) for each electrochemical process was calculated using eqn (9):

$$\Delta G = \Delta E + \Delta E_{ZPE} - T\Delta S \quad (9)$$

where the values of ΔE, ΔE_{ZPE}, and ΔS denote the changes in the DFT energy, the zero-point energy, and the entropy at 298 K, respectively.

Conflicts of interest

There are no conflicts to declare.

Acknowledgements

This research was also supported by a JSPS KAKENHI Program (grant no. 20H02568). This work was also supported by CREST (grant no. JPMJCR18R3) of the Japan Science and Technology Agency (JST). Synchrotron radiation experiments were performed using the BL01B1 Beam Line of SPring-8 with the approval of the Japan Synchrotron Radiation Research Institute (JASRI; Proposal Nos. 2017A1790, 2018A1349, 2019A1394, 2019B1159, 2020A1254 and 2020A1426). We express gratitude to Prof Y. Aso and Dr S. Tamba for his kind support in the synthesis of 2,2-bipyridine-5,5′-diamine.

Notes and references

1 S.-Y. Ding and W. Wang, *Chem. Soc. Rev.*, 2013, **42**, 548.
2 X. Feng, X. Ding and D. Jiang, *Chem. Soc. Rev.*, 2012, **41**, 6010.
3 J. L. Segura, M. J. Mancheno and F. Zamora, *Chem. Soc. Rev.*, 2016, **45**, 5635.
4 F. Vilela, K. Zhang and M. Antonietti, *Energy Environ. Sci.*, 2012, **5**, 7819.
5 S. Kandambeth, K. Dey and R. Banerjee, *J. Am. Chem. Soc.*, 2019, **141**, 1807.
6 E. Jin, J. Li, K. Geng, Q. Jiang, H. Xu, Q. Xu and D. Jiang, *Nat. Commun.*, 2018, **9**, 4143.
7 J. Lv, Y.-X. Tan, J. Xie, R. Yang, M. Yu, S. Sun, M.-D. Li, D. Yuan and Y. Wang, *Angew. Chem., Int. Ed.*, 2018, **57**, 12716.
8 J. Lee, O. Buyukcakir, T.-w. Kwon and A. Coskun, *J. Am. Chem. Soc.*, 2018, **140**, 10937.
9 C. Liu, W. Zhang, Q. Zeng and S. Lei, *Chem.–Eur. J.*, 2016, **22**, 6768.
10 G. Lin, H. Ding, R. Chen, Z. Peng, B. Wang and C. Wang, *J. Am. Chem. Soc.*, 2017, **139**, 8705.
11 D. Wang, Z. Zhang, L. Lin, F. Liu, Y. Wang, Z. Guo, Y. Li, H. Tian and X. Chen, *Biomaterials*, 2019, **223**, 119459.
12 M. Calik, F. Auras, L. M. Salonen, K. Bader, I. Grill, M. Handloser, D. D. Medina, M. Dogru, F. Loebermann, D. Trauner, A. Hartschuh and T. Bein, *J. Am. Chem. Soc.*, 2014, **136**, 17802.
13 K. Zhang, D. Kopetzki, P. H. Seeberger, M. Antonietti and F. Vilela, *Angew. Chem., Int. Ed.*, 2013, **52**, 1432.
14 X. Wang, L. Chen, S. Y. Chong, M. A. Little, Y. Wu, W.-H. Zhu, R. Clowes, Y. Yan, M. A. Zwijnenburg, R. S. Sprick and A. I. Cooper, *Nat. Chem.*, 2018, **10**, 1180.
15 K. Lei, D. Wang, L. Ye, M. Kou, Y. Deng, Z. Ma, L. Wang and Y. Kong, *ChemSusChem*, 2020, **13**, 1725.
16 H. B. Aiyappa, J. Thote, D. B. Shinde, R. Banerjee and S. Kurungot, *Chem. Mater.*, 2016, **28**, 4375.
17 S. M. J. Rogge, A. Bavykina, J. Hajek, H. Garcia, A. I. Olivos-Suarez, A. Sepulveda-Escribano, A. Vimont, G. Clet, P. Bazin, F. Kapteijn, M. Daturi, E. V. Ramos-Fernandez, F. X. L. i. Xamena, V. Van Speybroeck and J. Gascon, *Chem. Soc. Rev.*, 2017, **46**, 3134.
18 P. Su, K. Iwase, T. Harada, K. Kamiya and S. Nakanishi, *Chem. Sci.*, 2018, **9**, 3941.
19 W. Zhong, R. Sa, L. Li, Y. He, L. Li, J. Bi, Z. Zhuang, Y. Yu and Z. Zou, *J. Am. Chem. Soc.*, 2019, **141**, 7615.
20 K. Iwase, K. Kamiya, M. Miyayama, K. Hashimoto and S. Nakanishi, *ChemElectroChem*, 2018, **5**, 805.
21 O. Buyukcakir, S. H. Je, S. N. Talapaneni, D. Kim and A. Coskun, *ACS Appl. Mater. Interfaces*, 2017, **9**, 7209.
22 J.-D. Yi, R. Xu, Q. Wu, T. Zhang, K.-T. Zang, J. Luo, Y.-L. Liang, Y.-B. Huang and R. Cao, *ACS Energy Lett.*, 2018, **3**, 883.
23 J.-D. Yi, R. Xu, G.-L. Chai, T. Zhang, K. Zang, B. Nan, H. Lin, Y.-L. Liang, J. Lv, J. Luo, R. Si, Y.-B. Huang and R. Cao, *J. Mater. Chem. A*, 2019, **7**, 1252.
24 T. Li, C. Atish, K. Silambarasan, X. Liu and A. P. O'Mullane, *Electrochim. Acta*, 2020, **362**, 137212.
25 D. A. Popov, J. M. Luna, N. M. Orchanian, R. Haiges, C. A. Downes and S. C. Marinescu, *Dalton Trans.*, 2018, **47**, 17450.
26 E. M. Johnson, R. Haiges and S. C. Marinescu, *ACS Appl. Mater. Interfaces*, 2018, **10**, 37919.
27 S.-Y. Ding, J. Gao, Q. Wang, Y. Zhang, W.-G. Song, C.-Y. Su and W. Wang, *J. Am. Chem. Soc.*, 2011, **133**, 19816.
28 G. H. Gunasekar, K. Park, V. Ganesan, K. Lee, N.-K. Kim, K.-D. Jung and S. Yoon, *Chem. Mater.*, 2017, **29**, 6740.
29 R. Kamai, K. Kamiya, K. Hashimoto and S. Nakanishi, *Angew. Chem., Int. Ed.*, 2016, **55**, 13184.
30 R. Kamai, S. Nakanishi, K. Hashimoto and K. Kamiya, *J. Electroanal. Chem.*, 2017, **800**, 54.
31 K. Kamiya, R. Sugimoto, T. Tatebe, T. Harada and S. Nakanishi, *ChemSusChem*, 2020, **13**, 3462.
32 K. Kamiya, T. Tatebe, S. Yamamura, K. Iwase, T. Harada and S. Nakanishi, *ACS Catal.*, 2018, **8**, 2693.
33 K. Iwase, T. Yoshioka, S. Nakanishi, K. Hashimoto and K. Kamiya, *Angew. Chem., Int. Ed.*, 2015, **54**, 11068.
34 S. Kato, K. Iwase, T. Harada, S. Nakanishi and K. Kamiya, *ACS Appl. Mater. Interfaces*, 2020, **12**, 29376.
35 X. Zhao, P. Pachfule, S. Li, T. Langenhahn, M. Ye, C. Schlesiger, S. Praetz, J. Schmidt and A. Thomas, *J. Am. Chem. Soc.*, 2019, **141**, 6623.
36 R. Joseph Kline, M. D. McGehee and M. F. Toney, *Nat. Mater.*, 2006, **5**, 222.
37 G. K. Mor, O. K. Varghese, M. Paulose, K. Shankar and C. A. Grimes, *Sol. Energy Mater. Sol. Cells*, 2006, **90**, 2011.

38 R. K. Yadav, A. Kumar, N.-J. Park, K.-J. Kong and J.-O. Baeg, *J. Mater. Chem. A*, 2016, **4**, 9413.
39 K. Kamiya, R. Kamai, K. Hashimoto and S. Nakanishi, *Nat. Commun.*, 2014, **5**, 5040.
40 D. Liu, X. Zhang, Z. Sun and T. You, *Nanoscale*, 2013, **5**, 9528.
41 X. Huang, S. Tang, X. Mu, Y. Dai, G. Chen, Z. Zhou, F. Ruan, Z. Yang and N. Zheng, *Nat. Nanotechnol.*, 2011, **6**, 28.
42 X. Kong, K. Xu, C. Zhang, J. Dai, S. Norooz Oliaee, L. Li, X. Zeng, C. Wu and Z. Peng, *ACS Catal.*, 2016, **6**, 1487.
43 J. W. Hong, Y. Kim, D. H. Wi, S. Lee, S.-U. Lee, Y. W. Lee, S.-I. Choi and S. W. Han, *Angew. Chem., Int. Ed.*, 2016, **55**, 2753.
44 X. Zhang and Y. Xie, *Chem. Soc. Rev.*, 2013, **42**, 8187.
45 C. S. Diercks, S. Lin, N. Kornienko, E. A. Kapustin, E. M. Nichols, C. Zhu, Y. Zhao, C. J. Chang and O. M. Yaghi, *J. Am. Chem. Soc.*, 2018, **140**, 1116.
46 T. Sick, A. G. Hufnagel, J. Kampmann, I. Kondofersky, M. Calik, J. M. Rotter, A. Evans, M. Doeblinger, S. Herbert, K. Peters, D. Boehm, P. Knochel, D. D. Medina, D. Fattakhova-Rohlfing and T. Bein, *J. Am. Chem. Soc.*, 2018, **140**, 2085.
47 K. Takada, R. Sakamoto, S.-T. Yi, S. Katagiri, T. Kambe and H. Nishihara, *J. Am. Chem. Soc.*, 2015, **137**, 4681.
48 R. Sakamoto, K. Hoshiko, Q. Liu, T. Yagi, T. Nagayama, S. Kusaka, M. Tsuchiya, Y. Kitagawa, W.-Y. Wong and H. Nishihara, *Nat. Commun.*, 2015, **6**, 6713.
49 D. Zhu, Q. Zhao, G. Fan, S. Zhao, L. Wang, F. Li and J. Chen, *Angew. Chem., Int. Ed.*, 2019, **58**, 12460.
50 B. Zhang, S. Wang, W. Fan, W. Ma, Z. Liang, J. Shi, S. Liao and C. Li, *Angew. Chem., Int. Ed.*, 2016, **55**, 14748.
51 N. T. Hong Trang and K. Ishii, *J. Phys. Chem. C*, 2018, **122**, 3539.
52 Y. Sun, L. Han and P. Strasser, *Chem. Soc. Rev.*, 2020, **49**, 6605.
53 L. Guo, K. Liang, K. Marcus, Z. Li, L. Zhou, P. D. Mani, H. Chen, C. Shen, Y. Dong, L. Zhai, K. R. Coffey, N. Orlovskaya, Y.-H. Sohn and Y. Yang, *ACS Appl. Mater. Interfaces*, 2016, **8**, 34970.
54 M. Jakešová, D. H. Apaydin, M. Sytnyk, K. Oppelt, W. Heiss, N. S. Sariciftci and E. D. Głowacki, *Adv. Funct. Mater.*, 2016, **26**, 5248.
55 S. Calabrese Barton, J. Gallaway and P. Atanassov, *Chem. Rev.*, 2004, **104**, 4867.
56 K. Dey, M. Pal, K. C. Rout, S. Kunjattu H, A. Das, R. Mukherjee, U. K. Kharul and R. Banerjee, *J. Am. Chem. Soc.*, 2017, **139**, 13083.
57 M. A. Khayum, S. Kandambeth, S. Mitra, S. B. Nair, A. Das, S. S. Nagane, R. Mukherjee and R. Banerjee, *Angew. Chem., Int. Ed.*, 2016, **55**, 15604.
58 Q. Hao, C. Zhao, B. Sun, C. Lu, J. Liu, M. Liu, L.-J. Wan and D. Wang, *J. Am. Chem. Soc.*, 2018, **140**, 12152.
59 S. Kandambeth, B. P. Biswal, H. D. Chaudhari, K. C. Rout, S. Kunjattu H, S. Mitra, S. Karak, A. Das, R. Mukherjee, U. K. Kharul and R. Banerjee, *Adv. Mater.*, 2017, **29**, 1603945.
60 K. Iwase, S. Nakanishi, M. Miyayama and K. Kamiya, *ACS Appl. Energy Mater.*, 2020, **3**, 1644.
61 A. R. Millward and O. M. Yaghi, *J. Am. Chem. Soc.*, 2005, **127**, 17998.
62 D. B. Shinde, H. B. Aiyappa, M. Bhadra, B. P. Biswal, P. Wadge, S. Kandambeth, B. Garai, T. Kundu, S. Kurungot and R. Banerjee, *J. Mater. Chem. A*, 2016, **4**, 2682.
63 V. Hayez, A. Franquet, A. Hubin and H. Terryn, *Surf. Interface Anal.*, 2004, **36**, 876.
64 L. L. Jensen, J. T. Muckerman and M. D. Newton, *J. Phys. Chem. C*, 2008, **112**, 3439.
65 F. Tran and P. Blaha, *J. Phys. Chem. A*, 2017, **121**, 3318.
66 M. Shukla, N. Srivastava, S. Saha, T. R. Rao and S. Sunkari, *Polyhedron*, 2011, **30**, 754.
67 H. Irie, K. Kamiya, T. Shibanuma, S. Miura, D. A. Tryk, T. Yokoyama and K. Hashimoto, *J. Phys. Chem. C*, 2009, **113**, 10761.
68 T. Tatebe, T. Harada, K. Kamiya and S. Nakanishi, *Photochem. Photobiol. Sci.*, 2018, **17**, 1153.
69 C. M. Cardona, W. Li, A. E. Kaifer, D. Stockdale and G. C. Bazan, *Adv. Mater.*, 2011, **23**, 2367.
70 P. Makula, M. Pacia and W. Macyk, *J. Phys. Chem. Lett.*, 2018, **9**, 6814.
71 Y. Zhao, H. Liu, C. Wu, Z. Zhang, Q. Pan, F. Hu, R. Wang, P. Li, X. Huang and Z. Li, *Angew. Chem., Int. Ed.*, 2019, **58**, 5376.
72 J. Chen, X. Tao, C. Li, Y. Ma, L. Tao, D. Zheng, J. Zhu, H. Li, R. Li and Q. Yang, *Appl. Catal., B*, 2020, **262**, 118271.
73 D. Wang, C. Ao, X. Liu, S. Fang, Y. Lin, W. Liu, W. Zhang, X. Zheng, L. Zhang and T. Yao, *ACS Appl. Energy Mater.*, 2019, **2**, 6497.
74 S. Barazzouk, P. V. Kamat and S. Hotchandani, *J. Phys. Chem. B*, 2005, **109**, 716.
75 H. Li, W. Tu, Y. Zhou and Z. Zou, *Adv. Sci.*, 2016, **3**, 1500389.
76 T. Ozaki, *Phys. Rev. B*, 2003, **67**, 155108.
77 T. Ozaki and H. Kino, *Phys. Rev. B*, 2004, **69**, 195113.
78 K. Kamiya, *Chem. Sci.*, 2020, **11**, 8339–8349.

